Study of Heat Affected Zone (HAZ) in Thermit Welding Process

Ali. Moarrefzadeh

Abstract— **The thermal effect of Thermit welding that specially depends on the electrical arc and temperature field of it in workpiece, is the main key of analysis and optimization of this process, from which the main goal of this paper has been defined. Numerical simulation of welding process in SIMPELC method and by ANSYS software for gaining the temperature field of copper, the effect of parameter variation on temperature field and process optimization for different cases of Thermit are done. The influence of the welding parameter for each mode on the dimensions and shape of the welds and on their ferrite contents is investigated. Despite these simplifications, the model can be used to analyze the thermal conditions during thermit welding with sufficient accuracy. The predicted temperature history, weld deposit, and HAZ profiles were in good agreement with the experimental measurements in laboratory welds. It is found that the weld gap is the most influential welding parameter for rail thermit welding. A wider-gap weld appears to be less sensitive to chance variations in the other welding parameters, and therefore fairly consistent thermal conditions can be obtained.**

Keywords– Numerical Simulation, Thermit, FSI, SIMPLEC, Temperature Field and Copper

I. INTRODUCTION

Thermit welding is a chemically reaction welding process. The weld joint is produced by pouring of superheated molten metal around the joint to be welded, applying with or without of pressure. Thermit welding basically called a mixture of finely divided metal oxide and a metal reducing agent as aluminium.

Thermit welding principle: The necessary heat for joining metal of thermit welding is obtained from chemical reaction of metal oxide and metal reducing agent. Usually iron oxide is used as a metal oxide and aliminium or magnesium is used as metal reducing agent. The strong chemical attraction of aluminium for oxygen is the basis for thermit process. First the thermit mixture is ignited by a burning magnesium ribbon. The ignited temperature of thermit is about 12000C. When ignited in one spot of mixture, the heat reaction spreads through the mass. The aluminium merging with the oxygen of metal oxide and setting free the iron, which is deposited on joint portion into the mold as a highly superheated liquid metal. If theoretical temperature is about 30000C of thermit, due to chilling effect of crucible the temperature is reduced about 25000C. So it is sufficient for welding temperature.

Faculty member of Department of Mechanical Engineering, Mahshahr Branch, Islamic Azad University , Mahshahr , Iran. E-mail: a_moarrefzadeh@yahoo.com, a.moarefzadeh@mahshahriau.ac.ir , Tel: +989123450936

The thermit reaction is required about thirty second to ignite and it is non-explosive process. Thermit material is a mechanical mixture of metallic aluminum and processed iron oxide. Molten steel is produced by the reaction in a magnetite-lined crucible.

At the bottom of the crucible, a magnetite stone is burned, into which a magnetite stone thimble is fitted. This thimble provides a passage through which the molten steel is discharged into the mold. The hole through the thimble is plugged with a tapping pin, which is covered with a fire-resistant washer and refractory sand. The crucible is charged by placing the correct quantity of thoroughly mixed material in it. In preparing the joint for welding, the parts to be welded must be cleaned, aliened, and held firmly in place.

If necessary, metal is removed from the joint to permit a free flow of the metal into the joint. A wax pattern is then made around the joint in the size and shape of the intended weld.

A mold made of refractory sand is built around the wax pattern and joint to hold the molten metal after it is poured.

The sand mold is then heated to melt out the wax and dry the mold. The mold should be properly vented to permit the escape of gases and to allow the proper distribution of the metal at the joint. Welding crucible and mold is shown in Fig. 1.

II. HEAT TRANSFER MODEL OF THERMIT WELDING

Two pieces of slide-on welding mould surround the butted rail ends to form a welding cavity. After securing the mould and sealing the gap between rail and mould, the rail ends and weld mould are preheated with a propane–oxygen flame, and then molten steel is poured into the cavity to fuse the rail ends together. A heat transfer model was developed to analyze thermal history during this process using FIDAP, a finite-element analysis package from Fluent. Because of the complex nature of thermite welding, it is difficult to include all the physical phenomena in one model.

In this study, only heat conduction, which has the dominant influence on the temperature evolution in thermit welds, was modeled explicitly.

The differential Equations (1) – (6) are solved iteratively by the SIMPLEC numerical procedure:

Mass continuity equation:

$$\frac{1}{r}\frac{\partial}{\partial r}(r\rho\upsilon_r)+\frac{\partial}{\partial z}(\rho\upsilon_z)=0 \qquad (1)$$

Radial momentum conservation equation:

$$\frac{1}{r}\frac{\partial}{\partial r}(r\rho\upsilon_r^2)+\frac{\partial}{\partial z}(\rho\upsilon_r\upsilon_z)= -\frac{\partial\rho}{\partial r}-j_zB_\theta+\frac{1}{r}\frac{\partial}{\partial r}(2r\eta\frac{\partial\upsilon_r}{\partial r})+ \frac{\partial}{\partial z}(\eta\frac{\partial\upsilon_r}{\partial z}+\eta\frac{\partial\upsilon_z}{\partial r})-2\eta\frac{\upsilon_r}{r^2} \quad (2)$$

Axial momentum conservation equation:

$$\frac{1}{r}\frac{\partial}{\partial r}(r\rho\upsilon_r\upsilon_z)+\frac{\partial}{\partial z}(\rho\upsilon_z^2)= -\frac{\partial\rho}{\partial z}+j_rB_\theta+\frac{\partial}{\partial z}(2\eta\frac{\partial\upsilon_z}{\partial z})+ \frac{1}{r}\frac{\partial}{\partial r}(r\eta\frac{\partial\upsilon_r}{\partial z}+r\eta\frac{\partial\upsilon_z}{\partial r}). \quad (3)$$

Energy conservation equation:

$$\frac{1}{r}\frac{\partial}{\partial r}(r\rho\upsilon_r h)+\frac{\partial}{\partial z}(\rho\upsilon_z h)= \frac{1}{r}\frac{\partial}{\partial r}(\frac{rk}{c_p}\frac{\partial h}{\partial r})+\frac{\partial}{\partial z}(\frac{k}{c_p}\frac{\partial h}{\partial z})+ j_rE_r+j_zE_z-R, \quad (4)$$

Conservation of thermal energy:

$$\frac{\partial}{\partial t}(\rho C_pT)+\frac{u}{r}\frac{\partial}{\partial r}(\rho C_prT)+w\frac{\partial}{\partial z}(\rho C_pT) =\frac{1}{r}\frac{\partial}{\partial r}(kr\frac{\partial T}{\partial r})+\frac{\partial}{\partial Z}(K\frac{\partial T}{\partial Z})-\frac{\Delta H}{C_P}\frac{\partial F_L}{\partial t} \quad (5)$$

Conservation of electrical charge:

$$\frac{1}{r}\frac{\partial}{\partial r}(\sigma r\frac{\partial\phi}{\partial r})+\frac{\partial}{\partial z}(\sigma\frac{\partial\phi}{\partial z})=0 \quad (6)$$

In the solution of Equation (1) – (6), special attention needs to be put on the energy effects on the electrode surface. At the cathode surface, additional energy flux terms should be included in Eq. (4) because of thermionic cooling due to the mission of electrons, ion heating, and radiation cooling.

III. NUMERICAL SIMULATION

Finite elements simulations are done in 3 steps with the main pieces:

1- Modeling by FEMB
2- The thermal study and processing
3- Post-Processing result of analysis by ANSYS software for results discussion

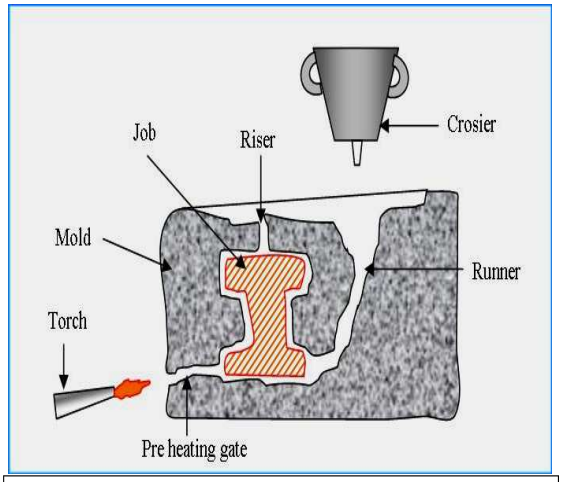

- Heat source
  - chemical reaction between thermit mixture components
  - Iron oxide and aluminium powder
  - ignition fuse required
- Fireclay mould
  - shapes joint
  - allows slag removal

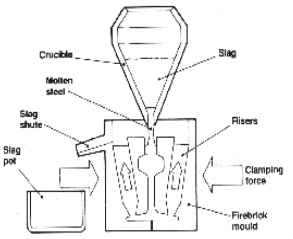

Fig. 1. Thermit Welding Process

Finite-Element techniques:

1-Finite elements modeling, types and properties for model different parts.
2- The definition of material properties
3- parameter definition
4- Loading
5- Boundary and initial value definition

IV. MODEL GENERATION

Because of the mirror symmetries about the longitudinal and transverse central planes, only one quarter of the weldment needs to be modeled. The model geometry that includes the shape of the rail, the weld, and the sand mould was built and meshed using GAMBIT, a preprocessor for FIDAP (Fig. 1). The actual dimensions of rail and mould were measured from a 136 lb rail and a standard Thermit SkV_ mould. The rail end was not fully covered by the mould in the model. A small portion of rail end passes beyond the mould collar and sticks into the weld chamber. This portion of rail end (referred to as 'stick-out' in Fig. 1) is subjected to the propane–oxygen flame during preheating and is surrounded by weld metal during solidification.

The amount of weld metal simulated in the model is the volume of weld cavity and is shaded in light grey in Fig. 1. As the dimensions of the weld mould are fixed for a given weld gap, the length of 'stickout' will affect the 'effective'

weld gap, which is the true distance between two butted rail ends.

An eight-node linear brick element was used to discredit the rail and part of the weld metal. The mesh density was uniform vertically from the rail head to base and gradually increased horizontally from the far end of the rail towards the weld end.

A four-node linear tetrahedron element was used to discretize the mould and the rest of weld metal (the geometry of which is more complicated). Again, the mesh density was higher in the weld metal and was gradually reduced in the mould with increasing distance from the weld–mould interface.

V. NUMERICAL CONSIDERATIONS

For the metal domain, the method developed by Torrey et al. was used to solve p, u, v, and T. This method is Eulerian and allows for an arbitrary number of segments of free surface with any reasonable shape. The basic procedure for advancing the solution through one time step, Dt, consists of three steps. First, explicit approximations to the momentum Equations (2) – (4) are used to find provisional values of the new time velocities at the beginning of the time step. Second, an iterative procedure is used to solve for the advanced time pressure and velocity fields that satisfy Eq. (1) to within a convergence criterion at the new time. Third, the energy equation Eq. (5) is solved. Fig.3. shows A typical sequences of temperature, electrical potential, and pressure distributions on the symmetric plane for an axisymmetric stationary arc.

For the arc plasma domain, a fully implicit formulation is used for the time-dependent terms, and the combined convection/ diffusion coefficients are evaluated using an upwind scheme. The SIMPLEC algorithm is applied to solve the momentum and continuity Equations (1) – (5) to obtain the velocity field. At each time step, the current continuity equation Eq. (6) is solved first, based on the updated parameters.

The new distributions of current density and electromagnetic force are then calculated for the momentum and energy equations. The momentum equations and the mass continuity equation are then solved in the iteration process to obtain pressure and velocity. The energy equation is solved to get the new temperature distribution. Next, the temperature-dependent parameters are updated, and the program goes back to the first step to calculate the current continuity equation. This process is repeated for each time step until the convergence criteria are satisfied.

A study of the influence of the electrode diameter on melting rate substitutes, with some authors, for a study of the influence of welding current density. This substitution is possible in order to perform a super®cial estimation, but in an accurate analysis, particularly in submerged arc welding, such a substitution is not allowable. Welding current is conducted through the wire extension also on its surface. In submerged arc welding, where the wire is dipped into flux during welding, this plays an important part. The experimental results regarding the influence of the electrode diameter on melting rate are shown in Figs. 3 and 4. Even an inaccurate estimation of the influence of the electrode diameter on the melting rate shows that this is a rational fractional function and that the number of wires used has no important influence on the form of functional relation. In twin-wire electrode welding (3 mm wire), melting rate is by 30±35% lower than with a 1.2 mm wire with equal current intensity per wire.

VI. BOUNDARY AND INITIAL CONDITIONS

The process of thermit rail welding was divided into two stages in the simulation, i.e. the preheating and tapping stage and the solidification stage. Different initial and boundary conditions were supplied forb each stage.

The solidification stage encompasses the time period after liquid metal is introduced into the weld cavity. The initial temperature field for the rail and the mould was obtained from the preheating and tapping simulation. The initial liquid temperature was determined from the peak temperature measured in weld cavity, which varied vertically along the y-axis and horizontally along the x-axis (Fig. 2). It was assumed that no temperature gradient was present along the z-axis in the weld cavity because of the relatively small dimension of weld gap in this direction.

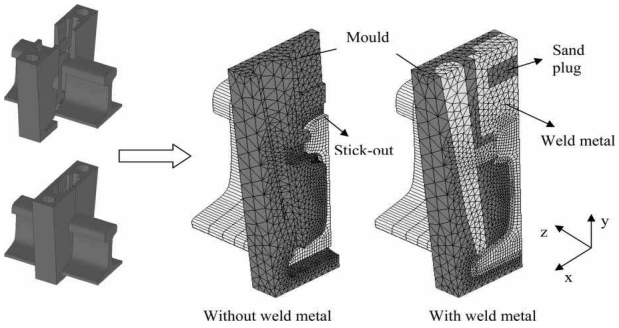

Fig. 2. Model with and without weld metal used in the simulations

Constant densities for the rail steel (7.87 g/cm3) and the sand mould (1.6 g/cm3) were assumed for the heat transfer simulations. The conductivities of the steel and the sand mould vary with temperature below the melting point, as shown in Fig. 3.

Weld deposit and HAZ profiles: Using the heat transfer model, isotherms of different temperatures can be obtained at any given time in a thermit weld. If a physical phenomenon has a certain characteristic temperature, the isotherm of this temperature can be used to represent the occurrence of this physical phenomenon. For example, if it is assumed that the liquid–solid interface has a certain temperature (solidus), then this isotherm can be plotted at different time steps to illustrate the dynamic motion of the solidification front. The furthest location the isotherm of solidus moves into the rail is therefore the profile of weld deposit. Similarly, the profile of the HAZ (whose outermost boundary is denoted by the eutectoid temperature) can also be determined from the model.

To compare the predicted and the actual weld deposit and HAZ profiles, laboratory thermit welds were cut off from parent rail and sectioned longitudinally in the rail web and head and horizontally in the rail base, as shown in Fig. 4. The obtained plates were lightly etched with Nital (2 per cent nitric acid with ethanol). The profile of HAZ can be

readily viewed on the etched surface, but the contrast of weld deposit is relatively poor in some samples. A metallurgical surface finish would be required for a good observation of the profile of weld deposit. As the surface area of the sectioned rail plate is very large (more than 250 cm2 in the case of the longitudinally sectioned plate), the normal metallurgical polishing becomes time consuming. To characterize the weld deposit profile quickly, radiography is used to determine the boundary of a weld deposit. As indicated as solid lines and the observed weld deposit profile are highlighted by dashed lines. When the centerline of the predicted weld deposit profile was lined up with the estimated centerline on a radiograph, a fairly good match was found in most areas. Figure 5 shows the comparison of HAZ profiles in the same laboratory weld. Again, a good match was found between the observed and predicted weld profiles. Additional comparisons of weld deposit and HAZ profiles for other laboratory welds give similar results.

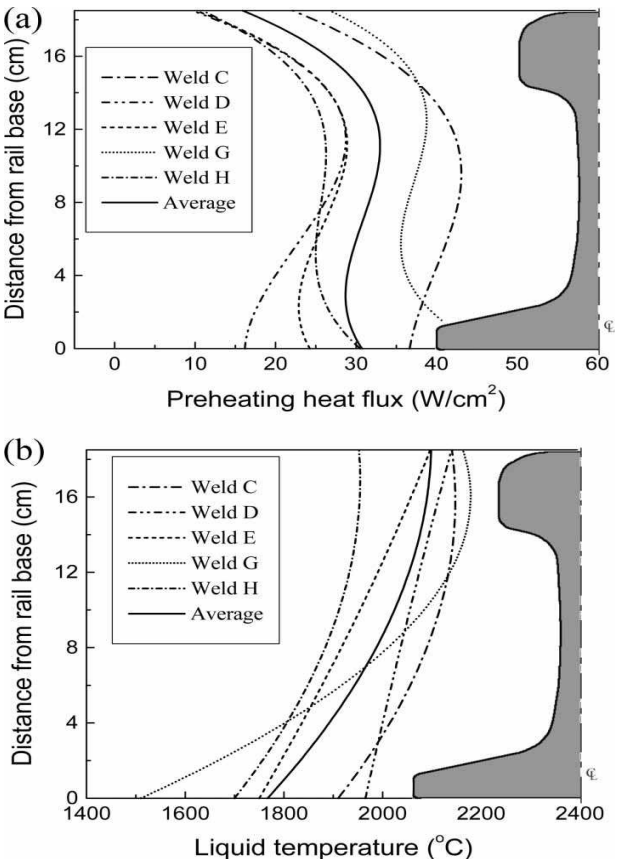

Fig. 3. (a) Preheating heat input and (b) initial liquid temperature used in simulations for laboratory thermit welds (weld F is not included in the averages)

VII. RESULT AND DISCUSIION

Conclusions for fluid temperature field copper temperature field, completely shown in Fig. 5.

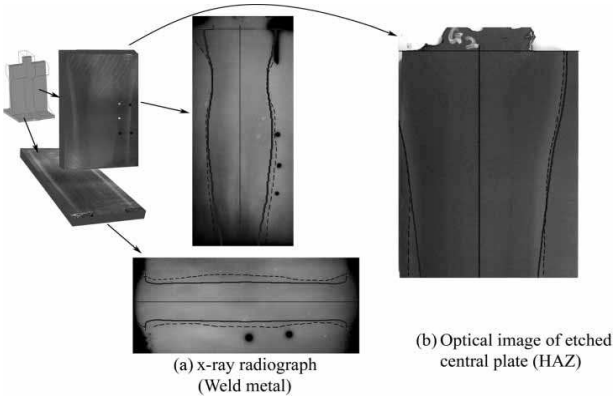

Fig. 4. (a) Comparison of the weld deposit profiles in the rail web and base for weld G; (b) comparison of the HAZ profiles in weld G (the dashed lines are the observation, and the solid lines are the predictions)

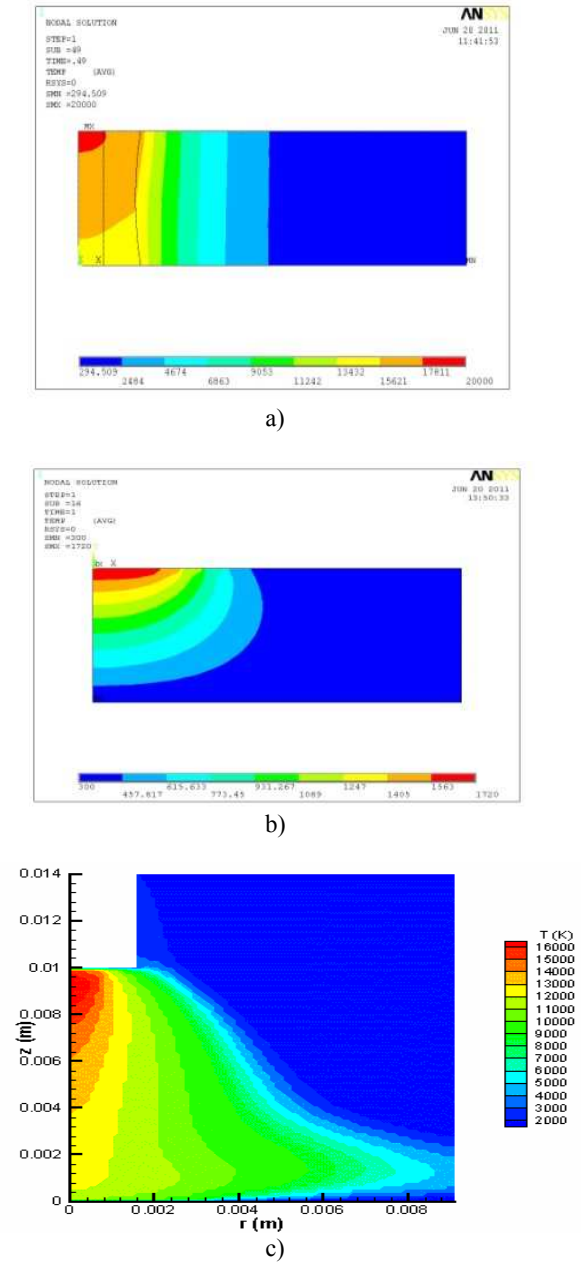

Fig. 5. Conclusions for temperature field: a) temperature field, b) Copper temperature field, c) Thermal profile of HAZ

VIII. CONCLUSIONS

1. A finite-element heat transfer model was developed for the standard thermit rail weld. The predicted temperature history curves were verified by temperature measurements in laboratory thermite welds. The heat transfer modeling results were also used to predict the weld deposit and the HAZ profiles. The predictions were in good agreement with the experimental observations.

2. Using both the temperature measurement and the thermal model, the preheating heat-input profiles were determined in laboratory thermit welds. The peak preheating heat flux was located in the rail web in most cases and occasionally in the

rail base. The preheating heat flux was found to vary considerably in different welds.

3. The liquid temperature distribution after pouring was determined from temperature measurements in weld cavity. An increasing liquid temperature from the rail base to the rail head was found in all laboratory welds.

A 3D mathematical model for the metal transfer process in thermit was formulated in this article. A complete model describing the Thermit welding process is developed, however, the computation of the transient solution of the complete model was prohibitively time-consuming and beyond the capability of the current PCs. In order to study the plasma arc interaction with metal during the metal transfer process, some simplifications have been made.

A case of an axisymmetric arc was studied first using this 3D model for the verification purpose. The numerical results agreed well with the previous two-dimensional studies. A case of a moving arc was then computed to demonstrate the 3D capability of the model.

REFERENCES

[1] S. Tashiro, M. Tanak, L. Murph, and J. Lowke, "Prediction of energy source properties of free-burning arc" Welding Journal, March 2008, pp. 23-29.

[2] A. Moarrefzadeh, "Numerical simulation of temperature field by Plasma arc welding Process in stainless steel" IREMOS Journal, February 2010, pp.101-107.

[3] A.Moarrefzadeh, "Choosing Suitable shielding gas for thermal optimization of GTAW process, IREME Journal, Sep 2010.

[4] E. Gorman, "New developments an application in plasma welding "Welding Journal, July 2004, pp. 547-556.

[5] Y. Wang, and Q. Chen, "On-line quality monitoring in Plasma arc welding" Journal of Materials Processing Technology, January 2005, pp. 270-274.

[6] H. Kyselica, "High–Frequency reversing arc switch for plasma welding of Aluminum" Welding Journal, May 2005, pp. 31-35.

[7] G. Langford, "Plasma keyhole arc welding of structural stainless steel joints" Welding Journal ,Feb2005, pp.102-113

[8] ANSYS Help system , Analysis Guide & Theory Reference Ver. 9,10

[9] H. Miller, "Automated GTA welding for aerospace fabrication ", Welding Journal, June 2005, pp. 439-501.

Ali Moarrefzadeh

Young Researchers Club, Mahshahr Branch, Islamic Azad University, Mahshahr, Iran

Faculty member of Department of Mechanical Engineering, Mahshahr Branch, Islamic Azad University , Mahshahr , Iran
E-mail: a_moarrefzadeh@yahoo.com
a.moarefzadeh@mahshahriau.ac.ir
Tel: +989123450936